

Spatially Averaged Flow Over a Wavy Surface

J. DUNGAN SMITH AND S. R. MCLEAN

Department of Oceanography, University of Washington, Seattle, Washington 98195

An understanding of the mechanics of nonuniform flow is important in a variety of ecological and geophysical fluid mechanical problems. Moreover, the ability to predict local boundary shear stress on an uneven bed is essential in erosion and sediment transport problems. In order to elucidate the important fluid mechanical phenomena active over natural quasi-two-dimensional bed forms a series of detailed flow measurements were made above 60- to 100-m-long 1- to 3-m-high dunes in the Columbia River. In this paper, velocity profiles obtained by averaging these flow data along lines of constant distance above the riverbed are examined, and it is shown that they can be constructed from well-known uniform flow results used in conjunction with a hypothesis about the structure of internal boundary layers. This approach permits skin friction as well as total boundary shear stress, averaged over one wavelength of the bed form, to be determined from spatially averaged velocity profiles and, conversely, provides a mechanism whereby zero-order velocity profiles can be constructed for two-dimensional nonuniform channel flows. Corrections for changes in the bottom roughness parameter caused by bed load transport and for flow stratification induced by suspended load transport are derived and applied in order to make the results consistent with the measured spatially averaged shear stress field.

INTRODUCTION

The beds of rivers and estuaries as well as those on continental shelves are rarely planar, and the presence of small-scale bottom topography creates pressure gradients in the flow that distort the velocity field near the boundary. In many physical oceanographic investigations these effects can be ignored; however, in sediment transport studies an accurate knowledge of the flow in the immediate vicinity of the bed is essential, and these effects are of primary importance. Unfortunately, not a great deal is known about the structure of turbulent velocity fields over nonplanar boundaries. Some theoretical investigations oriented toward the wind wave and sand wave generation problems have been carried out, and several inconclusive sets of laboratory data exist for flow over sinusoidal boundaries. However, much of this work examines the most easily linearizable aspects of the problem and concentrates on the case in which the fluid depth is large in comparison to the wavelength of the topography; important aspects of the problem do not yield to simple linearizations, and the Fourier components of natural topography do not always satisfy this criterion. In order to gain some insight into the character of large-scale finite depth nonuniform flow a series of experiments was carried out over a dune field in the Columbia River between 1968 and 1972.

The site of the investigation was the Bonneville Reservoir near Hood River, Oregon. As it cuts through the Cascades, the Columbia River is confined to a relatively narrow gorge, and the presence of the Bonneville Dam has little effect on the character of the high discharge flow through the reservoir. Moreover, during spring runoff, daily flow and power production associated discharge adjustments at the dam are relatively small, a nearly constant depth and steady ambient flow thus being guaranteed. This is important because the local depth was measured in relation to the free surface and the spatially dependent velocity field was measured from a bottom-mounted frame moved 3 m in the downstream direction every hour or so. Aanderaa current meters moored in the channel confirmed that the flow was steady. Riverbed and suspended sediment samples were collected at a number of stations, and

accurate maps were made of the bottom topography at various intervals throughout the studies.

Altogether, four field studies over seven sand waves were undertaken. During the first study, mean velocity was measured at four elevations in the boundary layer, and the boundary shear stress profile was obtained with a 4-cm-diameter Preston tube [see *Nece and Smith, 1970; Smith, 1970*]. Unfortunately, flow at the bottom current meter was disturbed by the Preston tube support, so in the following year the velocity field in the boundary layer was examined in greater detail from a more suitable frame at the expense of Preston tube measurements. By 1971, considerable information had been obtained on the mean velocity field, and the main effort was to be oriented toward elucidation of the Reynolds stress field. However, the flow was higher during the 1971 experiment, and the character of the sand wave field had changed, so emphasis again was placed on procurement of mean flow data. Although some Reynolds stress measurements were also made, this aspect of the program was not successful. Finally, in June 1972 a full set of mean velocity and Reynolds stress data was obtained from a substantially improved frame.

The current meters employed in this investigation were 4-cm-diameter mechanical velocity component sensors capable of resolving oscillations in excess of 5 Hz. Their precision was substantially better than 0.1 cm/s, and they were calibrated to this accuracy. However, in the two earlier experiments the flow measurements were degraded by an order of magnitude owing to the poor quality of the recording equipment that was available for use by the project at that time. In 1971, two accurate 14-track FM tape recorders and 15 pulse counters were employed, and by 1972 the flow measuring system was controlled with a Nova 1200 computer. *Smith [1974]* presents a discussion of the computer-based data recording system as well as details of the current meter design and calibration. Also, *J. D. Smith et al. (unpublished manuscript, 1976)* and *McLean [1976]* give further details on the experimental and data analysis techniques employed in the four Columbia River experiments.

The type and quality of data collected during each of the four Columbia River sand wave studies are summarized in Table 1. The four columns in this table represent (1) boundary

TABLE 1. Nature and Quality of Flow Measurements Obtained Over Seven Sand Waves in the Bonneville Reservoir of the Columbia River Between 1968 and 1972

Transect	1	2	3	4
1968 W1	good	poor	none	none
1969 W1	none	good	fair	none
1969 W2	none	fair	poor	none
1969 W3	none	good	fair	none
1971 W1	none	good	none	poor
1971 W2	none	good	none	poor
1972 W1	none	excellent	excellent	good

The columns represent (1) boundary shear stress measurements made with a Preston tube, (2) mean velocity measurements procured from a bottom-mounted frame, (3) mean velocity measurements made in the interior of the water column from a suspended frame, and (4) Reynolds stress profiles obtained by using the bottom-mounted frame. The last three types of measurements were made with the 4-cm-diameter mechanical velocity component sensing current meters described in the text.

shear stress measurements made with the large Preston tube described by *Nece and Smith* [1970], (2) boundary layer mean velocity profiles procured from a bottom-mounted frame, (3) mean velocity measurements made in the interior of the water column from a suspended frame, and (4) Reynolds stress measurements obtained near the riverbed from instruments mounted on the bottom frame. The investigations of specific waves are denoted as transects and are grouped in the left-hand column by years. The terms poor, fair, good, and excellent are relative but can be related to the overall measurement accuracy in a satisfactory manner. In particular, excellent is used to denote measurements made from a stable frame to the accuracy of the current sensor (approximately ± 0.1 cm/s). The term good is used to denote measurements that were recorded to the accuracy of the current meter but that were contaminated slightly by frame motion or occasional bursts of electronic noise. These are accurate to within a fraction of a centimeter per second. Fair is used to denote measurements that were contaminated by larger-amplitude frame motions, electronic noise, and poor recording equipment; they may contain errors of a few centimeters per second. This relative scale is concerned with the basic accuracy of the flow sensing and recording system. Interpretation of what the sensor measures or whether the full fluid mechanical regime has been resolved is not included. In the Columbia River experiments reported herein, the former was not a problem, and errors due to somewhat limited coverage of the complex nonuniform flow have been reduced substantially by spatially averaging the data.

FORMULATION OF THE PROBLEM

In order to determine a zero-order profile to use in perturbation theories for finite depth nonuniform flow the actual velocity field can be averaged over one wavelength along lines of constant distance from the boundary. This approach assigns all of the important nonlinear effects due to second- and higher-order terms to the zero-order profile and improves the accuracy of any theory that goes only to first order. However, to be of general value, a precise means of computing this zero-order profile in a specified situation is required.

When a momentum defect is produced by an obstacle in a turbulent flow, it diffuses outward with distance downstream

at a momentum-conserving rate, and when the flow field is averaged in the downstream direction, the velocity profile is more convex than would otherwise be the case. Near the boundary, there is a similarity region in which the velocity field is related to the local skin friction, whereas at great distances from the boundary, there is a similarity region in which the velocity field is related to the overall boundary shear stress, that is, to the boundary shear stress averaged over a large region of the bed, form drag on the topographic features thus being included. Roughness parameters for the two layers also differ, the one for the innermost region being associated with the sediment grains or the thickness of the bed load transport layer if bed material is in motion and the one for the outer region being related to the height and wavelength of the largest bed forms.

Usually, the riverbed or seabed is covered with ripples and dunes of discrete wavelengths, and in this situation the velocity field is analogously layered. The velocity scale for each layer is the shear velocity based on skin friction and form drag from the bed irregularities of the associated scale and smaller. In general, this is neither the actual shear stress at the boundary nor the stress in the zone of interest but rather the hypothetical boundary shear stress that would exist were the stress in the zone of interest extrapolated to the boundary by using steady uniform flow principles. If all of the topographic features of the bed produce matching levels of less than $0.2h$, where h is the flow depth, then the velocity in each region varies logarithmically with height, and the hypothetical boundary shear stresses can be determined from the slopes of the semi-logarithmic profiles. Under these circumstances the actual values of the shear velocity u_* and the roughness parameter z_0 can be determined for each layer from a least squares fit of u against $\log z$ using a straight line. In contrast, if one or more of the matching levels exceeds $0.2h$ in height, then the situation is more complicated, and the full velocity profile for a steady uniform flow must be used in the upper layers.

An eddy viscosity profile for a turbulent boundary layer is presented by *Hinze* [1959, p. 493] on the basis of data of

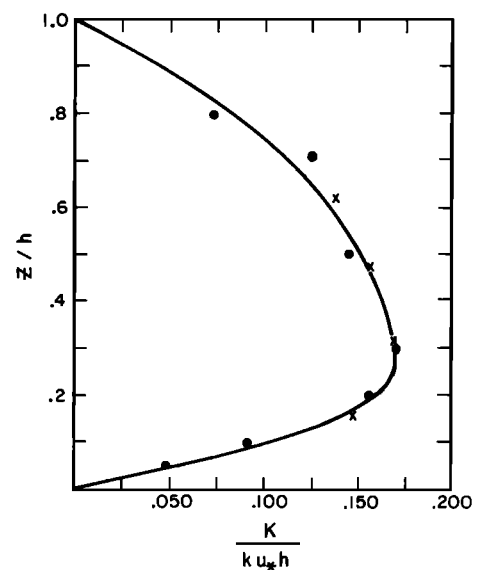


Fig. 1. Normalized eddy viscosity profile according to the data of *Townsend* [1951] (crosses) and *Klebanoff* [1954] (solid circles). Both sets of data were obtained from boundary layers rather than from channel flow, but the general shape of the curve appears to be universal. The solid curve is that given by (1).

Klebanoff [1954] and Townsend [1951]. Setting this eddy diffusion coefficient for momentum to zero at the free surface and fitting the experimental information with a two-part polynomial having four free coefficients in each part permit the construction of a continuous eddy viscosity field. Our fit is compared to the data of Klebanoff and Townsend, as plotted by Hinze [1959], in Figure 1; the resulting expression is

$$K/ku_*h = (\xi + 1.32892\xi^2 - 16.86321\xi^3 + 25.22663\xi^4) = f_2(\xi) \quad \xi_0 \leq \xi \leq 0.3 \quad (1)$$

$$K/ku_*h = (0.160552 + 0.075605\xi - 0.1305618\xi^2 - 0.1055945\xi^3) = f_1(\xi) \quad 0.3 \leq \xi \leq 1$$

where $\xi = z/h$ is the distance from the boundary divided by the flow depth. According to these data, von Karman's constant k is 0.40, but in light of the recent controversy over its exact value in geophysical scale flows [Businger *et al.*, 1971; Businger, 1973] it has been removed from (1) and left to be determined by the field data.

Using this information in conjunction with the linear stress profile that is required by the momentum equations in a uniform channel flow permits computation of a velocity field that is valid throughout the entire depth. Denoting this curve as $P(z/h, z_0/h) = P(\xi, \xi_0)$ and noting that the complete velocity field is given by $u = u_*P(\xi, \xi_0)$ permit u_* and z_0 to be determined from data over any reasonable depth range in any uniform flow, not just in the logarithmic region near the bed. In the problem at hand our hypothesis is that the velocity field acts as it would in a steady uniform flow, at least in the center of each layer; thus the above-mentioned hypothetical shear velocities and the roughness parameters can be determined by using the generalized profile function in each layer as long as it is thick enough.

SPATIALLY AVERAGED VELOCITY PROFILES

During the 1968 and 1969 experiments, discharge of the Columbia River at the Dalles Dam was about 8000 m³/s, whereas in the 1971 study it was 13,500 m³/s and in 1972 it was nearly 17,000 m³/s. During the 1968 and 1969 investigations, flow speeds 1 m from the seabed at the experimental sites were about 50 cm/s, whereas during the 1971 and 1972 experiments the current velocity magnitude at this level was about 82 cm/s. Under the conditions of the first two experiments, sediment was being transported at a low rate as bed load, but in the last two experiments, suspended load transport also occurred. Because of the predominance of bed load transport in the first two experiments the sand waves were relatively steep and very asymmetric, flow separation thus occurring just downstream

of their crests. In contrast, during the 1971 and 1972 studies, higher suspended load transport rates caused the sand waves to be more elongated for their height and more symmetrical, an unseparated flow situation resulting in spite of the relatively higher velocities. In the first case the ratio of wavelength to height ranged from 25 to 27, whereas in the second it ranged from 46 to 61; the actual values for each wave or transect are shown along with other pertinent geometric and flow parameters in Table 2. Therefore of the seven waves studied during the four studies, separation occurred in four cases and did not in three.

In the four experiments, flow data were collected at various distances from the seabed at a large number of positions over each sand wave, the details being described by J. D. Smith *et al.* (unpublished manuscript, 1976). In order to examine the zero-order velocity profile, data for each distance above the seabed at each station were averaged for 30 min or longer and then averaged together for every station along each transect. Subsequently, the downstream-averaged data were normalized by the flow speed 1 m from the seabed and plotted on two different graphs so that the separated and unseparated flow situations could be treated independently. Results from the two most accurate separated flow situations as indicated by Table 1 are shown in Figure 2a, and those from all of the unseparated flow cases are shown in Figure 2b. In both profiles, momentum defect zones associated with form drag on the sand waves are clearly shown in the immediate vicinity of the riverbed. Moreover, comparison of the 1969 and 1971-1972 profiles indicates a much higher drag associated with the latter in spite of the lower more rounded profile of the sand waves during these 2 years.

In the case of the separated flow measurements the slightly greater variance in the immediate vicinity of the seabed is due to the above-mentioned use of a less accurate data recording system, and the data points for locations more than 3 m above the riverbed were somewhat further degraded by employing a frame designed for boundary layer use but suspended from a cable above the riverbed. In 1972 an interior flow frame that permitted the current meters to be mounted on the axis of rotation was used in the upper part of the water column, eliminating such errors. Nevertheless, all of the data presented in Figure 2 are well within the accuracy required to resolve the phenomena of concern in this paper and to evaluate the five coefficients of Table 3 and the next two sections of this paper with reasonable accuracy.

THEORETICAL CONSIDERATIONS

In erosion problems it is very important to be able to separate skin friction from the spatially averaged boundary shear

TABLE 2. Geometric Parameters for the Larger Dunes on Each Transect and Flow Velocity 100 cm From the Seabed

Transect	h , m	λ_2 , m	H_2 , m	λ_2/H_2	λ_2/h	H_2/h	u_{100} , cm/s
1968 W1	13.4	81.0	3.21	25.2	6.04	0.24	53.86
1969 W1	15.9	74.3	2.74	27.1	4.69	0.17	42.83
1969 W2	16.3	67.0	2.62	25.6	4.11	0.16	51.83
1969 W3	16.6	82.0	3.16	26.0	4.94	0.19	49.20
1971 W1	14.5	82.0	1.34	61.2	5.66	0.09	84.72
1971 W2	14.3	80.0	1.66	48.2	5.59	0.12	80.97
1972 W1	15.0	96.0	2.07	46.4	6.40	0.14	82.52

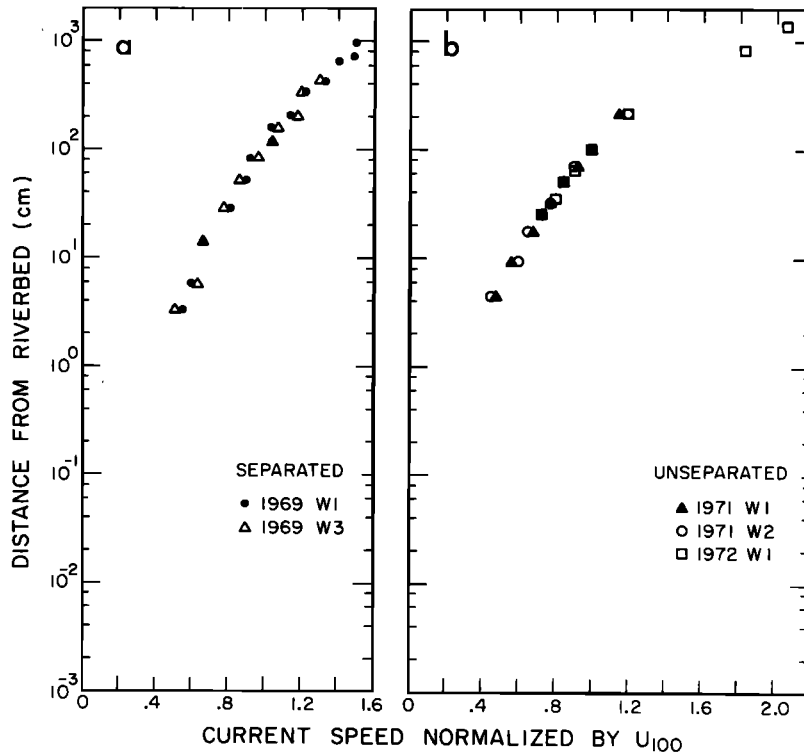


Fig. 2. Normalized spatially averaged profiles for flow over a sand wave field in the Columbia River: (a) measurements over asymmetrical dunes above which the flow separated and (b) measurements over three waves of a more sinusoidal character above which the flow did not separate. Note the general convex shape of the profiles caused by large-scale bed forms.

stress that includes form drag due to topographic features, because only the former is related to the sediment transport process. Although a sound procedure based on fundamental fluid mechanical principles has been unavailable for this purpose to date, it is likely that one can be constructed through careful analysis of the F_0 profiles presented in Figure 2. In attempting to do so the flow must be divided into layers. At least in the lower part of each layer the velocity field is given by

$$u = [(u_*)_n/k] \ln [z/(z_0)_n] \quad (2)$$

where $(u_*)_n$ is the friction velocity and $(z_0)_n$ is the roughness parameter for that zone. Equating expressions for two successive layers at the matching height $(z_*)_{n, n+1}$ and rearranging give the desired ratio of shear velocities as

$$\frac{(u_*)_n}{(u_*)_{n+1}} = \frac{\ln [(z_*)_{n,n+1}/(z_0)_{n+1}]}{\ln [(z_*)_{n,n+1}/(z_0)_n]} \quad (3)$$

where $n + 1$ is the outer of the two layers; however, for this equation to be of any value, relationships for $(z_*)_{n, n+1}$, $(z_0)_n$, and $(z_0)_{n+1}$ in terms of known parameters are required.

In an investigation of the form drag exerted by Arctic winds on sea ice, Arya [1975] equates z_* with the height of the internal boundary layer formed downstream of each pressure ridge and employs a relationship derived by Elliot [1958] to find this height. In the notation of this paper the thickness of the internal boundary layer, according to Elliot, is given by

$$(\delta_0)_{n,n+1}/(z_0)_n = a_0(x/(z_0)_n)^{4/5} \quad (4)$$

where x is the distance downstream and a_0 is a constant ranging from 0.6 to 0.9. In his calculations, Arya takes λ_* as the spacing of the obstacles and sets $(z_*)_{n,n+1} = (\delta_0)_{n,n+1}$ at $x =$

λ_* . However, in the F_0 profiles at hand the matching level must be more closely associated with the average height of the internal boundary layer, so

$$\frac{(z_*)_{n,n+1}}{(z_0)_n} = \frac{(\delta_{av})_{n,n+1}}{(z_0)_n} = \frac{a_0}{\lambda} \int_0^\lambda \left[\frac{x}{(z_0)_n} \right]^{4/5} dx = a_1 \left[\frac{\lambda}{(z_0)_n} \right]^{4/5} \quad (5)$$

where λ is the wavelength of the dunes and $a_1 = 5a_0/9$ ranges from 0.3 to 0.5. The approach to be used here is analogous to that followed by Arya [1975] but not identical, primarily because the problem being addressed is somewhat different. In particular, the zero-order flow in the Columbia River is of finite depth, the fluid mechanical conditions at the origin of the internal boundary layer are not well defined, and the topographic feature causing the momentum defect is the same scale as the distance between obstacles. For these reasons, a_1 may deviate from the value given by Elliot's theory, and in particular, it is likely to be slightly lower.

In nonsediment-transporting flows over sand beds the value of z_0 for the bottommost layer is obtained from the well-known curve of Nikuradse [1933], reproduced, for example, by Schlichting [1968, p. 583], but for river flow in which sediment transport is active, no general procedure for computation of z_0

TABLE 3. Experimentally Determined Coefficients for the Zero-Order Velocity Profile Theory

	α_0	a_1	γ_1	k	C_D
Separated flow	26.3	0.0995	1.24×10^{-3}	0.38	0.212
Unseparated flow	26.3	0.0995	1.24×10^{-3}	0.38	0.840

has been suggested. However, in a paper on the bed load transport of noncohesive sediment by wind, *Owen* [1964] suggests that the roughness parameter $(z_0)_b$ is related to the height of the bed load layer when the sediment transport is by saltation. Balancing the potential energy at the top of the particle trajectory with its maximum kinetic energy, *Owen* finds the thickness of the saltation layer to be $\rho_s u_0^2 / [2(\rho_s - \rho)g]$, where ρ_s is the density of the sediment grains, ρ is the density of the transporting fluid, u_0 is the maximum vertical velocity of the saltating particle, and g is the acceleration due to gravity. In the case of sediment transport by wind, ρ is much less than ρ_s , so the densities cancel from this expression. *Owen* then argues that u_0 must be proportional to u_* and writes $z_0 \propto u_*^2 / (2g)$. Using the experimental data of *Chepil* [1945a, b, c], *Zingg* [1953], and *Bagnold* [1941], he finds the constant of proportionality to be about 2.07×10^{-2} .

If z_0 is related to the thickness of the saltation layer when sediment is being transported by wind, then an analogous relationship must exist for bed load transport by water; however, a direct application of *Owen's* [1964] expression in the latter case leads to values of z_0 of the order of 10^{-5} cm, and his argument that the initial particle velocity is proportional to the local shear velocity needs to be reexamined. Instead of relating u_0 to u_* it would be more reasonable to argue that the initial kinetic energy of the sedimentary particle is proportional to the force exerted on the grain as it leaves the bed times the distance over which it accelerates, that is, the work done on the grain when it is removed from the boundary. This change in the derivation makes no difference to *Owen's* final result if the force on the particle goes as $\tau_b D^2$, where D is the grain diameter, but does mean that a factor of $\rho / (\rho_s - \rho)$ has been included in the empirically derived constant. Moreover, it is likely that the force on the particle, thus the work done per unit volume in lifting it from the riverbed or seabed, is scaled by $\tau_b - \tau_c$, where τ_c is the critical boundary shear stress associated with the initiation of sediment motion. When this approach is taken, a general expression of the form

$$z_0 = z_N \quad \tau_b < \tau_c \quad (6a)$$

$$z_0 = \alpha_0(\tau_b - \tau_c) / [(\rho_s - \rho)g] + z_N \quad \tau_b \geq \tau_c \quad (6b)$$

can be found. Here z_N is the z_0 given by *Nikuradse's* [1933] work and has been included so that (6) can be used for very low sediment transport rates where the first term is small. If τ_c is neglected, *Owen's* [1964] work yields $\alpha_0 = 22.8$, whereas using the Columbia River data with τ_c included gives $\alpha_0 = 26.3$.

The values of z_0 for all layers except the bottom one can be specified in terms of drag coefficients. As used for form drag only, the drag equation provides a relationship between the force arising from a pressure distribution on the surface of an obstacle and the flow that would exist in the neighborhood of the obstacle in its absence. In the case of a two-dimensional bed form the force per unit width is given by

$$F_D = \rho(C_D/2)U_r^2 H \quad (7)$$

where H is the height of the topographic feature and U_r is the appropriate reference velocity. As U_r is associated with the undisturbed flow, it must be related to the inner velocity profile, but it also determines the value of z_0 in the outer layer, so the only acceptable reference point is the matching level between the inner and the outer layer. It should be noted that the height of this reference point and the flow there can be written entirely in terms of inner layer parameters and those associated with the bed form geometry. Writing $F_D = (\tau_{n+1} -$

$\tau_n)\lambda$ and substituting the appropriate version of (2) into (7) yield

$$\tau_{n+1} - \tau_n = \frac{\rho C_D}{2} \left[\frac{(u_*)_n}{k} \ln \frac{(z_*)_{n,n+1}}{(z_0)_n} \right]^2 \frac{H_{n+1}}{\lambda_{n+1}} \quad (8)$$

Substitution from (5) yields

$$\frac{\tau_{n+1} - \tau_n}{\tau_n} = \frac{C_D}{2k^2} \frac{H_{n+1}}{\lambda_{n+1}} \left[\ln a_1 \left(\frac{\lambda_{n+1}}{(z_0)_n} \right)^{4/5} \right]^2 \quad (9)$$

and rearranging gives

$$\frac{\tau_{n+1}}{\tau_n} = 1 + \frac{C_D}{2k^2} \frac{H_{n+1}}{\lambda_{n+1}} \left[\ln^* a_1 \left(\frac{\lambda_{n+1}}{(z_0)_n} \right)^{4/5} \right]^2 \quad (10)$$

so

$$\frac{(u_*)_{n+1}}{(u_*)_n} = \left\{ 1 + \frac{C_D}{2k^2} \frac{H_{n+1}}{\lambda_{n+1}} \left[\ln a_1 \left(\frac{\lambda_{n+1}}{(z_0)_n} \right)^{4/5} \right]^2 \right\}^{1/2} \quad (11)$$

Now the ratio of shear velocities can be found directly from (11) when a_1 , C_D , k , the apparent bed roughness $(z_0)_n$, and the geometry of the bed forms are specified. Equation (3) is used in conjunction with this ratio and with (5) to compute $(z_0)_{n+1}$. Therefore in a neutrally stable spatially averaged flow all parameters of interest can be calculated for a particular flow and set of bed forms once the constants a_1 , k , and C_D are set for each general class of bed form problems.

SUSPENDED SEDIMENT INDUCED FLOW STRATIFICATION

In flow over an erodible bed containing materials for which the ratio of particle settling velocity to local shear velocity is small, sediment will diffuse from the neighborhood of the boundary to the interior of the fluid and will be transported there in the suspended mode. This causes the sediment concentration to decrease with distance into the flow, producing a stably stratified boundary layer. The net fluid density ρ_f is related to the volume concentration of suspended sediment ϵ_s by

$$\rho_f = \rho + (\rho_s - \rho)\epsilon_s \quad (12)$$

so the density gradient is related to the concentration gradient by

$$(\partial \rho_f / \partial z) = (\rho_s - \rho)(\partial \epsilon_s / \partial z) \quad (13)$$

and the gradient Richardson number can be written as

$$R_t = \left[\frac{-g}{\rho} \frac{\partial \rho_f}{\partial z} \right] \left(\frac{\partial u}{\partial z} \right)^{-2} = \left[\frac{-(\rho_s - \rho)g}{\rho} \frac{\partial \epsilon_s}{\partial z} \right] \left(\frac{\partial u}{\partial z} \right)^{-2} \quad (14)$$

This parameter measures the importance of flow stratification in inhibiting the turbulent transfer of momentum and mass, turbulence production being completely eliminated above the critical value of 0.25 or so.

In investigations of the lower part of the atmospheric boundary layer it is usual to assume a constant stress region in which the nondimensional shear is

$$\phi_m = (kz/u_*)(\partial u / \partial z) \quad (15)$$

and in a stably stratified case this is related to the gradient Richardson number by

$$\phi_m = 1 + \beta(z/L) = (1 - \alpha \beta R_t)^{-1} \quad (16)$$

Here α is the ratio of the eddy diffusivity of mass to that of momentum, β is a constant found to be 4.7 ± 0.5 by *Businger et al.* [1971],

$$L = \rho u_*^3 / gk \Theta_0 \quad (17)$$

is the Obukhov length, and Θ_0 is the density flux in the lowest part of the fully turbulent layer.

Equations (15) and (16) have been shown to be valid in constant stress and constant buoyancy flux layers, but it is likely that they can be generalized. Nondimensionalizing the one-dimensional constitutive equation $\tau = \rho K(\partial u / \partial z)$ by the boundary shear stress yields for a channel flow

$$(K/u_*^2)(\partial u / \partial z) = \tau / \tau_b = 1 - \xi \quad (18)$$

When (16) is used, the following analogous expression can be written for the constant stress layer:

$$[ku_*z(1 - \alpha\beta R_i)/u_*^2](\partial u / \partial z) = 1 \quad (19)$$

Comparison of (18) for $\xi \ll 1$ and (19) gives

$$K = ku_*z(1 - \alpha\beta R_i) \quad (20)$$

In contrast, if $R_i = 0$, then K in (18) is given by (1) throughout the entire fluid, so the simplest general form that the eddy viscosity can have is

$$K = ku_*hf_2(\xi)(1 - \alpha\beta R_i) \quad (21)$$

where $f_2(\xi) \rightarrow \xi$ as $\xi \rightarrow 0$. Although in general f_2 may depend on $\alpha\beta R_i$ in some complicated inseparable fashion and simplify to (20) only as the boundary is approached, there is no evidence that this is the case, and for the present it seems reasonable to postulate that (21) is valid throughout the flow. In addition, it should be noted that in sediment transport problems the region of greatest interest, thus that requiring the greatest computational accuracy, is in the immediate vicinity of the bed and no error is incurred by the generalization there.

The relationship between $\zeta = z/L$ and R_i used in (16) is strictly valid only for a Richardson number defined in a constant buoyancy flux layer; however, it is unlikely that the expression will depend upon the mechanism causing the stratification as long as it has been parameterized properly, and it is postulated here that (16), for the constant stress layer, and (21) are of general validity, that is, they can be used with the R_i of (14) even though the diffusive sediment flux varies with distance from the boundary and is balanced by an advective flux at every level.

In steady horizontally uniform flow, conservation of mass gives

$$K_s(\partial \epsilon_s / \partial z) + w_s \epsilon_s(1 - \epsilon_s) = 0 \quad (22)$$

where K_s is the diffusion coefficient for sediment and w_s is the settling velocity of the sediment particles. When the diffusion coefficients for sediment and momentum are equated in the constant stress layer to give $\alpha = 1$ and $K_s = ku_*z$, (22) can be integrated to yield

$$\frac{\epsilon_s}{1 - \epsilon_s} = \frac{\epsilon_a}{1 - \epsilon_a} \left(\frac{z_a}{z} \right)^p \quad (23)$$

where ϵ_a is the concentration at reference level z_a and $p = w_s/ku_*$. As $p \rightarrow 0$ in (23), $\epsilon_s \rightarrow \epsilon_a$, and as $p \rightarrow \infty$, $\epsilon_s \rightarrow 0$ except at z_a . The former limit is called wash load, whereas the latter is the bed load case, and the nature of this limit suggests that z_a should be taken to be the top of the bed load layer δ_b . Noting that δ_b is proportional to $\alpha_0(\tau_b - \tau_c)/[(\rho_s - \rho)g]$ according to the arguments leading to (6) and taking this unknown constant of proportionality to be unity specify z_a . Typically, $z_a \gg z_N$ in a bed load transport situation, so $z_a \approx z_0$. The fact that δ_b may

be $10z_0$ or so is not of concern as long as ϵ_a is computed at z_a from measurements made above δ_b , as is inevitably the case.

Smith [1977] suggests that ϵ_a can be written in terms of a maximum permissible concentration ϵ_0 and the normalized excess shear stress $s = (\tau_b - \tau_c)/\tau_c$ in the form

$$\epsilon_a = \epsilon_0 \gamma_0 s / (1 + \gamma_0 s) \quad (24)$$

where γ_0 is an empirical constant of the order of 10^{-3} . This expression gives $\epsilon_a \rightarrow \epsilon_0$ as $s \rightarrow \infty$ and reduces to $\epsilon_a = \gamma_1 s$ when $\gamma_1 s = \epsilon_0 \gamma_0 s \ll 1$, the latter approximation being in general agreement with available low-concentration bed load and suspended load theories. Suspended sediment measurements made approximately 10 cm above the riverbed during the 1971 and 1972 Columbia River sand wave experiments yield $\gamma_1 = 1.24 \times 10^{-8}$ when z_a is specified as described in the previous paragraph, and for $\epsilon_0 = 0.65$ this yields $\gamma_0 = 1.95 \times 10^{-3}$. The constants γ_0 and γ_1 were calculated on the basis of the measured concentration 10 cm from the bed with the assumption that all of the sediment was of a single size class. In reality, the bed was composed of a distribution of sediment sizes with a mean diameter of 0.27 mm ($\phi = 1.875$). As the finer particles are more readily diffused into the interior, their contribution to the density stratification becomes relatively more important with distance from the bed. For this reason the suspended sediment was assumed to be all of size $\phi = 2.5$. This provides a reasonable estimate of the stratification effect away from the bed but introduces some error very close to the bottom, where a significant amount of coarse material is present as well. To eliminate this error, the concentration must be calculated to include all the different sediment sizes. This requires generalization of (24) and subsequent adjustment of γ_0 so that the calculated profile still matches the measured suspended sediment concentration at 10 cm. Recently, Smith and McLean [1977] have carried out the more general computations and found a value of $\gamma_0 = 2.4 \times 10^{-3}$.

In the problem at hand, (14), (18), (21), and (22) are coupled and must be solved simultaneously in order to obtain the actual velocity and suspended sediment fields. The boundary conditions are

$$u = 0 \quad \text{at } z = z_0 \quad (25a)$$

$$\epsilon = \epsilon_a \quad \text{at } z = z_a \approx z_0 \quad (25b)$$

Combining (14) and (21) gives

$$\begin{aligned} K &= ku_*hf_2(\xi) \left[1 + \alpha\beta \left(\frac{\rho_s - \rho}{\rho} gh \frac{\partial \epsilon_s}{\partial \xi} \right) \left(\frac{\partial u}{\partial \xi} \right)^{-2} \right] \\ &= ku_*hf_2(\xi) \left[1 + \beta_* \left(\frac{\partial \epsilon_s}{\partial \xi} \right) \left(\frac{\partial u}{\partial \xi} \right)^{-2} \right] \end{aligned} \quad (26)$$

and using (26) with (18) yields

$$\frac{\partial u}{\partial \xi} = \frac{u_*}{k} \left[\frac{1 - \xi}{f_2(\xi)} \right] \left[1 + \beta_* \left(\frac{\partial \epsilon_s}{\partial \xi} \right) \left(\frac{\partial u}{\partial \xi} \right)^{-2} \right]^{-1} \quad (27)$$

Similarly, combining (26) and (22) gives

$$\frac{\partial \epsilon_s}{\partial \xi} = -p \epsilon_s (1 - \epsilon_s) \left\{ f_2(\xi) \left[1 + \beta_* \frac{\partial \epsilon_s}{\partial \xi} \left(\frac{\partial u}{\partial \xi} \right)^{-2} \right] \right\}^{-1} \quad (28)$$

or

$$\begin{aligned} \frac{\partial \epsilon_s}{\partial \xi} &= -p \left[\left(1 + \frac{\epsilon_s}{1 - \epsilon_s} \right)^{-2} \left(\frac{\epsilon_s}{1 - \epsilon_s} \right) \right] \\ &\quad \cdot \left\{ f_2(\xi) \left[1 + \beta_* \frac{\partial \epsilon_s}{\partial \xi} \left(\frac{\partial u}{\partial \xi} \right)^{-2} \right] \right\}^{-1} \end{aligned} \quad (29a)$$

and when (28) is integrated,

$$\frac{\epsilon_s}{1 - \epsilon_s} = \frac{\epsilon_a}{1 - \epsilon_a} \exp \left\{ -p \int_{\xi_a}^{\xi} \left[1 + \beta_* \frac{\partial \epsilon_s}{\partial \xi} \cdot \left(\frac{\partial u}{\partial \xi} \right)^{-2} \right]^{-1} \frac{d\xi}{f_d(\xi)} \right\} \quad (29b)$$

Now (27) in combination with (29a) and (29b) can be used as the basis of an iterative solution. As the first step in this process, take $\beta_* = 0$ in (27) and (29) to get the first estimates of $\partial u / \partial \xi$ and $\partial \epsilon_s / \partial \xi$, respectively. Next, use these two values in the right-hand sides of (27) and (29) to get new estimates, and continue the process until these parameters are known to the desired accuracy. Finally, the values of $\partial u / \partial \xi$ and $\partial \epsilon_s / \partial \xi$ can be substituted into the right-hand side of

$$u = \frac{u_*}{k} \int_{\xi_a}^{\xi} \frac{(1 - \xi)}{f_d(\xi)} \left[1 + \beta_* \frac{\partial \epsilon_s}{\partial \xi} \left(\frac{\partial u}{\partial \xi} \right)^{-2} \right]^{-1} d\xi \quad (30)$$

and (29) to get the velocity and sediment concentration profiles.

COMPARISON OF THEORY AND FIELD MEASUREMENTS

Solution of (27) and (29) with (1), (3), (4), (6), (11), (24), and (25) provides a complete description of both the velocity and the suspended sediment field when α_0 , a_1 , k , C_D , and γ_0 are specified. At first glance it appears as if these five parameters are available to use to improve agreement with two measured velocity profiles and a measured stress profile, and to some degree that assessment of the problem is correct. To this extent the general utility of the approach presented in this paper will depend upon its confirmation under other conditions. However, three of the coefficients that were used already were known with reasonable accuracy, and all were severely limited in the values that they could have taken on without making the approach suspect. For example, von Karman's constant must be between 0.35 and 0.41, and the numerical value for α_0 must be close to that obtained by Owen [1964]. These coefficients were specified from field data primarily because their exact values in a geophysical scale channel flow were not known with sufficient accuracy and the data set under present discussion afforded a chance to determine them. In the Kansas experiment described by Businger *et al.* [1971] an accurate determination of von Karman's constant gave a value of 0.35 rather than 0.40 as is typically quoted, so direct use of 0.40 in these experiments appeared unwarranted. Similarly, Owen [1964] points out that the value of his coefficient (related in a previous section to α_0) cannot be constant over a wide range of conditions, and it likewise seemed more reasonable to determine α_0 from the experimental data rather than to use a potentially incorrect value. The situation in regard to a_1 is somewhat analogous, and one might have proceeded by using the value given by Elliot [1958]; however, it seemed that in light of the differences between the present problem and that considered by Elliot an empirical determination of this parameter also was reasonable as long as it turned out to be of the order of but less than the predicted value. Moreover, in all three of these cases the final results are not particularly sensitive to small changes in the actual values.

There is no reason to believe that α_0 , γ_0 , k , or a_1 will differ significantly in analogous problems, and we consider their specification here similar to the determination of universal constants rather than a curve-fitting exercise. One possible exception is in regard to the drag coefficient. Although the

order of magnitude that this parameter must have is known, the specific value that is chosen has at least a moderate effect on the final shape of the curve, and the empirical determination of this parameter certainly improves the fit between theory and data. However, even here, more evidence for the specific values that have been chosen exists than at first meets the eye. There were two generations of sand waves in each of the experiments, and the drag coefficient was found to be the same for both sets of waves in each case to the accuracy with which the geometric parameters of the sand waves were known.

As was mentioned above, the parameters in Table 3 in combination with (1), (3), (4), (6), (11), (18), (22), (24), (25), (27), and (29) constitute a complete definition of the zero-order velocity and suspended sediment concentration profiles over a discrete spectrum of boundary roughnesses given one external flow parameter, the heights and wavelengths of the well-defined bed forms, and the sediment and fluid characteristics; however, in order to set the coefficients in this table an iterative approach was required. By examining Figures 2a and 2b carefully, layers were defined for each case. At first we implicitly assumed that the suspended sediment concentration was sufficiently small to be neglected and proceeded to fit $u = u_* P(\xi, \xi_0)$ to the data. The empirically determined u_* and z_0 in the layers next to the boundary were used to find α_0 , and the intersections between inner and middle and inner and outer layers were used to find a_1 .

Unfortunately, the exact nature of the outermost layer could not be specified accurately because the matching level was slightly above the position of the top current meter on the boundary layer frame; raising the matching level much above this point caused the drag coefficient to become unreasonably high, and lowering it below this point caused increasing disagreement between measured and computed velocity and stress fields. Therefore for the sake of simplicity the upper matching level was taken to be fixed at the level of the upper current meter on the boundary layer frame. The error introduced by this assumption is not likely to be very large, but it does cause an uncertainty of 10% or so in the evaluation of a_1 . When the analysis technique just described was used with a value of 0.40 for von Karman's constant, the predicted stress profile was systematically too high for the unseparated flow data, so to obtain reasonable agreement between velocity and stress fields, a value of 0.35 had to be used. However, this was found to degrade the fit substantially in the separated flow case in which a negligible amount of bed material was being transported in suspension, indicating that a stratification correction, due to the much greater suspended sediment concentrations present during the higher-discharge experiments, was required.

Subsequently, the theory of the previous section was developed and applied to the unseparated flow case. A value of 0.38 for von Karman's constant was found to be in good agreement with both 1969 and 1971-1972 results once a stratification correction had been applied to the latter. Also, the measured and computed velocity and stress profiles were put into good agreement when this technique was used.

In carrying out the least squares fit it was felt that the 1969 W1 and 1969 W3 data sets as well as the 1971 W1, 1971 W2, and 1972 W1 data sets were sufficiently close to each other that greater benefit was obtained by fitting them jointly than by treating them separately. In effect, this assumes that the sparseness of each individual data set degrades the fit more than the slight differences in geometric parameters between the

TABLE 4. Flow and Sediment Parameters for Each Transect

Transect	$(u_*)_0$, cm/s	z_N (for τ_c), cm	$(z_0)_0$, cm	ϵ_a	$(z_*)_{0,1}$ (log), cm	$(u_*)_1$, cm/s	$(z_0)_1$, cm	$(z_N)_{1,2}$ (log), cm	$(u_*)_2$, cm/s	$(z_0)_2$, cm	$(z_*)_{0,1}$ (actual), cm	$(z_*)_{1,2}$ (actual), cm	Variance, cm ² /s ²
1968 W1	2.92	9.26×10^{-4}	0.106	0.00544	21.9	3.83	0.379	109.7	5.33	1.87	24.7	113.4	37.32
1969 W1	1.69	9.26×10^{-4}	0.014	0.00101	14.7	2.53	0.141	84.0	3.67	1.03	14.0	103.7	2.39
1969 W2	2.74	9.26×10^{-4}	0.090	0.00463	21.2	3.63	0.345	92.5	5.00	1.58	20.7	113.9	9.68
1969 W3	2.32	9.26×10^{-4}	0.055	0.00296	19.2	3.17	0.266	103.2	4.49	1.54	18.8	112.4	2.27
1971 W1	4.64	9.08×10^{-4}	0.317	0.0157	10.7	6.80	0.972	133.7	9.98	4.66	62.9	198.2	1.92
1971 W2	4.44	9.08×10^{-4}	0.287	0.0142	10.5	6.58	0.929	129.9	10.35	5.61	50.5	184.3	1.36
1972 W1	4.52	9.08×10^{-4}	0.299	0.0148	10.6	6.68	0.946	150.9	10.79	6.55	53.3	217.8	13.90

various transects that were composited. The resulting fits are shown in Figure 3. In carrying out these regressions the values of α_0 , a_1 , γ_0 , and k were assumed to be independent of whether the flow separated over the topographic feature; however, it was assumed that the drag coefficient could differ between these two situations, and indeed the results indicate that it did.

As was mentioned previously, the suspended sediment field in the 1968 and 1969 experiments was negligible, whereas during the 1971 and 1972 investigations this was not the case. Fortunately, the flow speeds 100 cm from the riverbed that were used to normalize the flow data did not differ sub-

stantially in the three unseparated flow situations, so the same concentration profile could be used in each. This is shown on the right-hand side of Figure 3b. It should be noted from (22) and (26) that the slope of the concentration profile depends upon u_* and therefore changes from level to level. The value of u_* to be used in computing the excess shear stress is the one for the lowest layer.

Measured and theoretical shear stress profiles are shown in Figure 4. The most salient feature of this diagram is the increase in stress with distance from the boundary in the immediate vicinity thereof. This is caused by the z dependent

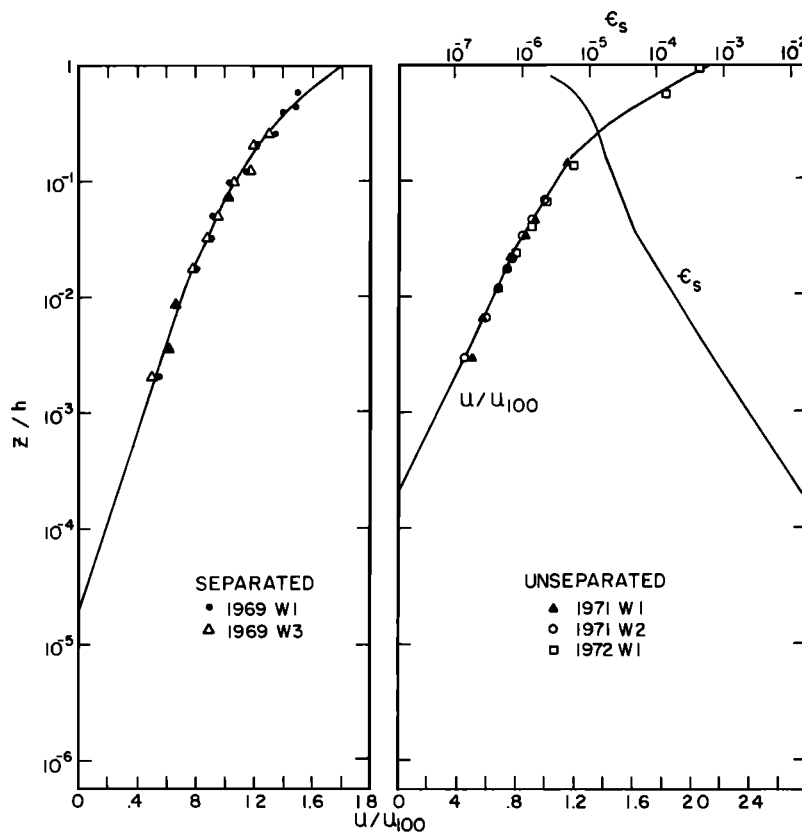


Fig. 3. Comparison of spatially averaged experimental and theoretical velocity profiles for flow over a sand wave field in the Columbia River: (a) results over steep asymmetrical waves above which flow separation occurred and (b) velocity field over more sinusoidal waves above which no flow separation occurred. The suspended sediment profile for the second case is shown on the right side of Figure 3b. The breaks in slope in the velocity and suspended sediment concentration profiles are due to changes in the scale velocities associated with the presence of dunes on the riverbed.

pressure gradient, due in turn to the presence of the topographic features. Note that the general features of the measured shear stress field are fairly well predicted by the simple theory, in spite of the additional constraint that the actual stress field must vary smoothly with distance from the boundary.

Because of the procurement of Reynolds shear stress profiles during the 1972 investigation the unseparated flow data set is more comprehensive, and for this reason it was analyzed first. It is possible to divide the plotted points shown in Figure 2b into three groups, those below about 50 cm, those between 50 and 220 cm, and those above 220 cm. Points in the lower two groups lie approximately on two logarithmic lines of different slope. However, for the sake of obtaining greater accuracy, segments of velocity profiles given by the generalized function P were fit in a least squares manner to each of the three groups of points. In doing this the measured Reynolds shear stress 35 cm from the bed (shown in Figure 4) was taken to approximate the boundary shear stress fixing u_* for the bottom region; then by trying different values of z_0 the best fit velocity profile was obtained. For each z_0 , velocity and suspended sediment concentration fields had to be computed by using (25), (27), and (29). Once the best fit velocity profile for the bottom region was found, α_0 and γ_0 were computed. The coefficient α_0 was calculated from (6) with z_0 and τ_b from the flow data and τ_c and z_N from the sediment parameters. Similarly, γ_0 was found from (24), τ_b , τ_c , and the apparent concentration of suspended sediment at z_0 being known.

For the middle of the three layers, u_* was chosen by taking the best fit linear stress profile $\tau = \tau_b(1 - \xi)$ through the Reynolds stress measurements at 100 and 214 cm. The analysis for this layer is similar to that of the lower layers. The concentration field was taken to be that which would exist in the absence of the lower and upper layers, but it was set equal to the concentration from the analysis for the lower layer at the matching level between the two regions. As (4) gives the matching level in the absence of stratification and because the actual matching level was unknown before the best fit to the middle region was calculated, a reasonable initial guess had to be employed. By taking the concentration at the estimated matching point from the profile for the lower region as the reference value, P , R_s , and ϵ_s were calculated iteratively, and the variance was minimized by varying z_0 . At this point a better estimate of the matching level was found, and the process was repeated until the desired accuracy was obtained. Once these iterations were completed, best fits for the lower and middle regions were available, and only the upper region remained undetermined. As was stated earlier, the matching level between the middle and the upper region was taken to be the level of the top current meter on the frame, the necessity of using iteration to find the matching point and hence the reference concentration for the uppermost region thus being eliminated. As was done before, the concentration field was assumed to be the one that would be present independent of the lower layers except for specification of the reference value at the matching level. Again various values of z_0 were tried in order to minimize the variance, but in this case the u_* was specified by z_0 and the velocity at the matching level as given by the velocity distribution for the middle level. The velocity field was computed once more by iteration between (25), (27), and (29), and the z_0 and u_* giving the minimum variance were found.

At this point, u_* and z_0 for each region were specified by the regressions. As the geometry of the large dune (which was

actually a composite feature constructed of segments of several dunes so that the data could be treated as an ensemble) in the 1972 experiment was well known, its height and wavelength were used to determine the drag coefficient from (11) and a_1 from (5). Both were calculated by using the log profile defined by u_* and z_0 , which represent the asymptotic behavior of the velocity in the unstratified limit as the boundary is approached. Through the application of these coefficients to the lower matching level, the height and wavelength of the smaller waves which were present on the back of the larger one were computed from (5) and (11) to be about 15 cm and 4.5 m, respectively. These smaller dunes appeared on the depth recorder, but their lengths and heights could not be resolved very accurately for reasons ranging from the presence of surface wind waves to the scale of the graphic readout on the Fathometer. Nevertheless, the computed values of these parameters were well within the ranges estimated from the echo sounding records (8–30 cm in height and 4.0–5.3 m in length).

In the separated flow case the boundary shear stress was sufficiently small to neglect flow stratification in the analysis. As was true before, three groups of data points could be discerned from Figure 2a, those below about 20 cm, those from 20 to 100 cm, and those above about 100 cm. Again best

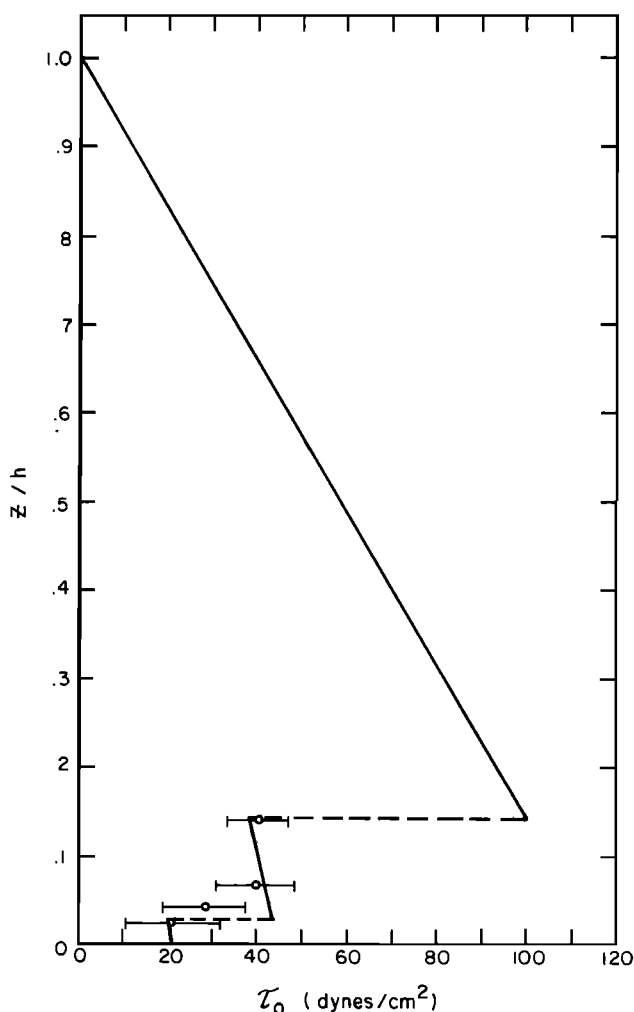


Fig. 4. Experimental and theoretical shear stress profiles. Note the increase in boundary shear stress with distance from the riverbed.

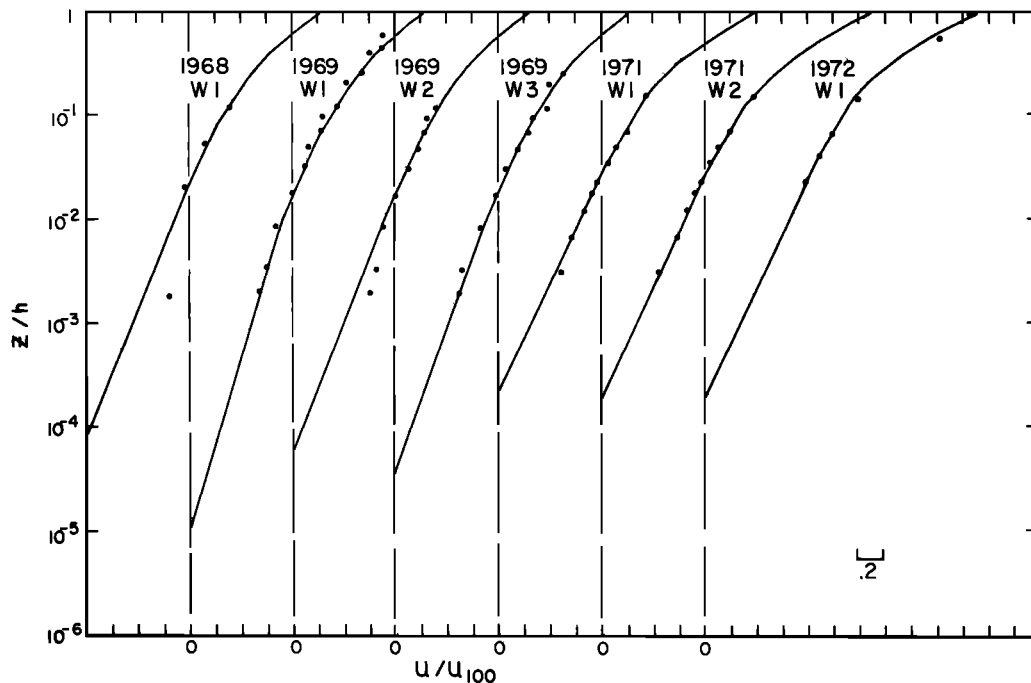


Fig. 5. Individual theoretical and experimental velocity profiles for flow over seven separate Columbia River sand waves measured during 4 different years. Note the reasonable agreement between experimental points and theoretical curves. The point nearest the riverbed for 1968 W1 was affected by the frame that it was mounted on and cannot be considered to be reliable.

fit velocity profiles satisfying certain constraints were compared to the data in each of the three regions; however, in this case the coefficients α_0 , a_1 , and k from the previous analysis were used. In the bottom region the variance of the data points around the integral of (18) with (1) was minimized by trying different values of z_0 , which in turn implicitly specified u_* , through (6). When the stratification effect were neglected, the only repeated computations were those required by changing z_0 .

For the middle region the minimum variance was achieved by again trying different values of z_0 , but in this instance, u_* was given by a least squares fit to the velocity profile. The wavelengths and heights of the large dunes were sufficiently similar and sufficiently well known to permit the matching level between the middle and the upper region to be determined from (5); with this information, u_* and z_0 were obtained by varying the latter until the minimum variance with respect to the data was achieved.

At this point it was possible to compute the drag coefficient for the upper region by using (11), for which the value of C_D is shown in Table 3. With this and a_1 it was possible to determine the height and wavelength of the smaller waves by using (5) and (11). These were found to be 50 cm and 14.6 m, respectively, and as was true in the previous case, the results are in good agreement with values estimated from echo sounding profiles.

Figure 5 shows the results of applying the complete theory with the coefficients of Table 2 to the seven individual transects made between 1968 and 1972. To use this information, one flow parameter must be specified, and in producing the profiles of Figure 5 a least squares fit to the data was used. However, the flow speed at a particular level or the discharge per unit flow width could just as well have been chosen for this purpose.

APPLICATION OF THE THEORY TO OTHER SITUATIONS

Owing to the nature of the analysis the proper procedure for computing the zero-order flow field in a given situation requires starting at the boundary and working out into the interior. Unfortunately, in most geophysical flow situations the parameters in the interior region are most easily measured or computed, so some sort of iterative approach is necessary. If $(u_*)_0$ is known or estimated, $(z_0)_0$ can be found from (6). However, if sediment is being transported by the flow, the value of α_0 given in Table 3 is required as well.

The top of the inner layer is determined through (5) by a_1 from Table 3, $(z_0)_0$, and the wavelength of the smallest bed forms. Next $(u_*)_1$ and $(z_0)_1$ are found by using (11) and (3), respectively, and the relevant parameters from Tables 2 and 3. If still larger bed forms are present, then more layers can be characterized in the same manner. Once $(u_*)_n$ and $(z_0)_n$ for each layer are known, it remains only to construct the actual velocity profiles. For the case, as was true in the 1968 and 1969 experiments, in which the stratification is negligible, the velocity is found by simply integrating (18) with (1) and (25a). The velocity profiles for each region are then linked together at the actual matching levels.

If as is the case in each of the experiments considered in this analysis, the actual boundary shear stress is not known, a scheme for finding it must be constructed. One method is to pick five initial estimates which span the realm of possibility. Therefore one of the three intermediate estimates generates the velocity profile which best satisfies the known flow conditions. It is now possible to try values midway between the best original estimate and the two estimates on either side defining another five-point grid which spans a smaller range of possibilities. A computer can then iteratively search for the $(u_*)_0$ which best satisfies the known flow data to a given accuracy.

For those cases in which the stratification effect due to suspended sediment is not negligible, the analysis is somewhat more involved because of the coupling of the velocity, concentration, and Richardson number fields. To calculate the actual velocity profile in the lowest region requires an iterative solution of (25), (27), and (29), which is most easily accomplished by initially assuming $R_i = 0$ and then solving the shear and concentration gradient fields and combining these to get a better estimate of the Richardson number.

The higher levels are complicated by the fact that the concentration field is dependent on the actual matching level, which is as yet unknown, introducing yet another iteration. This is accomplished by initially taking the reference concentration for the higher level to be that given by the analysis for the lower region at the log matching layer. This allows computation of an estimate of the actual matching level, which gives a better estimate of the reference concentration and its appropriate level. The process is repeated until the actual matching level is found to the desired accuracy. From the above description it can be seen that dealing with the stratification effect adds two levels of iteration to the analysis, but they are necessary, since the presence of suspended sediment can have a significant effect on the flow field. In the production of Figure 5, only three to five iterations were required to insure an error of less than 1%.

The smallest bed forms considered in this analysis have been tens of centimeters high and several meters long. In many situations involving transport of sand, ripples of a few centimeters in height and a few tens of centimeters in length develop. Because these were completely unresolvable on the depth recorder and because the velocity measurements were not made close enough to the bed to determine their effect, they were left out of the analysis. In the 1971 and 1972 experiments the sediment transport rate was probably high enough to have severely reduced the amplitude of or even eliminated the ripple field; however, in 1968 and 1969, ripples of a few centimeters in height were said to be present by divers. Proper inclusion of these features is impossible because their lengths and heights were not measured accurately; however, an additional layer with estimates of these parameters was included in the model, and the boundary shear stress was reduced only slightly. A larger effect does not occur because the high value for z_0 given by (6) is just below that due to the ripple field, so the ripples are ineffectual as form drag producing agents.

CONCLUSIONS

In this paper it has been shown that the spatially averaged velocity profile over a wavy boundary in a turbulent flow has a convex shape when it is plotted in a semilogarithmic manner and that the associated shear stress profile increases with distance from the boundary to a maximum at a position related primarily to the wavelength of the bottom topography and secondarily to the roughness of the boundary. The increasing shear stress zone is related to a z dependent pressure gradient caused in turn by the large-scale topographic features and not predicted by presently available perturbation theories. In addition, these experimental results are shown to be in agreement with a simple theoretical model based on an outwardly diffusing momentum defect zone. The model is directly applicable both to the flow of clear water over a fixed boundary and to sediment transport situations.

In order to treat the effects of bed load transport on the flow the semiempirical method by which Owen [1964] computes z_0 is generalized and shown to be in good agreement with the

measured data. The effects of suspended sediment induced stable stratification are also examined, and procedures to compute the associated reduction in eddy diffusivity based on standard atmospheric boundary layer methods are employed. However, these are altered to account for the absence of a constant flux zone, which in turn is caused by the settling of the sediment particles. The stratification in both the atmospheric and sediment transport situations is due to a density flux at the boundary. In the former the density anomaly diffuses through the layer with the fluid particles, whereas in the latter this is not the case because the suspended sedimentary material settles back toward the boundary. Moreover, in an equilibrium suspended sediment transport situation there is no density anomaly sink at great distances from the boundary, and a constant density flux cannot be maintained through the boundary layer. Therefore as the settling velocity becomes negligible and the sedimentary material becomes wash load, the density gradient disappears.

The suspended sediment induced stratification correction presented in this paper can also be used for a uniform channel flow; however, in the majority of natural sediment transport situations, quasi-two-dimensional bed forms develop on the channel bottom, and the complete theory presented in this paper is necessary for a proper resolution of the spatially averaged flow situation. Also, the approach presented here gives the ratio of skin friction to total boundary shear stress, as is required for application of bed load theories such as those of Yalin [1963] and Einstein [1950]. As a means for computing suspended sediment concentration profiles is given, the suspended sediment flux can be obtained easily by multiplying these two parameters together and integrating over the flow depth.

Finally, the model outlined in this paper provides, for the first time, a means for computing spatially averaged velocity profiles to be used in perturbation expansion type theories in order to compute the actual velocity field over irregular topography in nonrotating systems. This approach has the advantage of putting the essential nonlinearities into the zero order, thus permitting substantially more accurate flow fields to be determined from theories that only go to first order.

Although the procedures followed in this paper may seem at first glance to be fairly complicated, they are programmed and handled quite easily on most digital computers.

Acknowledgments. The work described herein was supported by National Science Foundation grants GA-14178 and DES-75-15154. Contribution 930 from the University of Washington, Seattle.

REFERENCES

- Arya, S. P. S., A drag partition theory for determining the large-scale roughness parameter and wind stress on the Arctic pack ice, *J. Geophys. Res.*, **80**, 3447-3454, 1975.
- Bagnold, R. A., *The Physics of Blown Sands and Desert Dunes*, Methuen, London, 1941.
- Businger, J. A., Turbulent transfer in the atmospheric surface layer, in *Workshop on Micrometeorology*, edited by D. A. Haugen, p. 67, American Meteorological Society, Boston, Mass., 1973.
- Businger, J. A., J. C. Wyngaard, Y. Izumi, and E. F. Bradley, Flux-profile relationships in the atmospheric surface layer, *J. Atmos. Sci.*, **28**(2), 181, 1971.
- Chepil, W. S., Dynamics of wind erosion, 1, Nature of movement of soil by wind, *Soil Sci.*, **60**(5), 305, 1945a.
- Chepil, W. S., Dynamics of wind erosion, 2, Initiation of soil movement, *Soil Sci.*, **60**(5), 397, 1945b.
- Chepil, W. S., Dynamics of wind erosion, 3, The transport capacity of the wind, *Soil Sci.*, **60**(6), 475, 1945c.
- Einstein, H. A., The bed load functions of sediment transportation in open channel flows, *U.S. Dep. Agr. Soil Conserv. Serv. Tech. Bull.* **1026**, 1-71, 1950.

- Elliot, W. P., The growth of the atmospheric internal boundary layer, *Eos Trans. AGU*, 38, 1048, 1958.
- Hinze, J. O., *Turbulence*, McGraw-Hill, New York, 1959.
- Klebanoff, P. S., Characteristics of turbulence in boundary layer with zero pressure gradient, *Nat. Adv. Comm. Aeronaut. Tech. Notes*, 3178, 1-56, 1954.
- McLean, S. R., Mechanics of the turbulent boundary layer over sand waves in the Columbia River, doctoral dissertation, Univ. of Wash., Seattle, 1976.
- Nece, R. E., and J. D. Smith, Boundary shear stress in rivers and estuaries, *J. Waterways Harbors Div. Amer. Soc. Civil Eng.*, 96(WW2), 335, 1970.
- Nikuradse, J., Strömungsgesetze in rauhen Röhren, *VDI Forschungsh.*, 361, Ausgabe B, 4, July/Aug. 1933.
- Owen, P. R., Saltation of uniform grains in air, *J. Fluid Mech.*, 20(2), 225, 1964.
- Schlichting, H., *Boundary Layer Theory*, 6th ed., McGraw-Hill, New York, 1968.
- Smith, J. D., Stability of a sand bed subjected to a shear flow of low Froude number, *J. Geophys. Res.*, 75(30), 5928, 1970.
- Smith, J. D., Turbulent structure of the surface boundary layer in an ice covered ocean, *Rapp. Proces Verb. Reunions Cons. Perma. Int. Explor. Mer*, 167, 53, 1974.
- Smith, J. D., Modeling of sediment transport on continental shelves, in *The Sea*, vol. 6, edited by E. D. Goldberg, John Wiley, New York, in press, 1977.
- Smith, J. D., and S. R. McLean, Boundary layer adjustments to bottom topography and suspended sediment, *Mem. Soc. Roy. Sci. Liege*, 11, in press, 1977.
- Townsend, A. A., The structure of the turbulent boundary layer, *Proc. Cambridge Phil. Soc.*, 47, 375, 1951.
- Yalin, M. S., An expression for bed-load transportation, *J. Hydraul. Div. Amer. Soc. Civil Eng.*, 89(HY3), 221, 1963.
- Zingg, A. W., Wind tunnel studies of movement of sedimentary material, *Stud. Eng. Bull.* 34, p. 111, Univ. of Iowa, Iowa City, 1953.

(Received March 15, 1976;
revised November 2, 1976;
accepted November 18, 1976.)